PROCEEDINGS OF THE SEVENTEENTH LUNAR AND PLANETARY SCIENCE CONFERENCE, PART 2
JOURNAL OF GEOPHYSICAL RESEARCH, VOL. 92, NO. B4, PAGES E617–E626, MARCH 30, 1987

Quantitative Abundance Estimates From Bidirectional Reflectance Measurements

JOHN F. MUSTARD AND CARLE M. PIETERS

Department of Geological Sciences, Brown University, Providence, Rhode Island

A simplified approach to the problem of determining the relative proportion of minerals in a mixture from a reflectance spectrum of the mixture is presented. Fundamental to this approach is a priori information concerning reflectance spectra of the minerals in the mixture and some estimate of the particle sizes of the mixture components. Reflectance spectra of intimate mixtures are a systematic but nonlinear combination of the spectra of the minerals in the mixtures. Equations for bidirectional reflectance are used to linearize the systematics of spectral mixing for intimate mixtures. The equations are simplified by assuming that particulate media scatter light isotropically at phase angles between 15° and 40°. This method for linearizing the mixing systematics is used to determine mineral relative geometric cross sections (proportional to mass fraction/density x particle diameter) from reflectance spectra of mixtures of igneous rock-forming minerals (olivine, magnetite, enstatite, and anorthite) and to determine endmember relative geometric cross sections from reflectance spectra of mixtures of terrestrial desert soils. Since particle diameters are known, the mass fractions of the mixture components are also calculated. For materials without strongly absorbing components, the accuracy of abundance determinations is better than 5%. The results indicate that the method presented can be used to accurately determine the relative proportions of components (minerals or complex endmembers) in a mixture from a reflectance spectrum of the mixture given information of the endmembers in the mixture, reflectance spectra of the endmembers, and an estimate of particle sizes of the respective mixture components.

INTRODUCTION

Reflectance spectra have been used for many years to obtain compositional information for planetary surfaces. At visible to near-infrared wavelengths, charge transfer, electronic transitions, and other electronic processes associated with transition metal ions (Fe, Ti, Cr, etc.) result in diagnostic absorptions [*Burns*, 1970; *Adams*, 1974, 1975]. In addition, bending, stretching, and other vibrational processes in molecules such as H_2O and OH^- produce fundamental and overtone absorptions in this same wavelength region [*Hunt and Salisbury*, 1970*a*]. The position, shape, and strength of these diagnostic absorptions are controlled by the particular crystal structure in which the absorbing species is contained and mineralogic information can be derived from the characteristics of the absorption bands in a spectrum.

Although reflectance spectra of a variety of minerals have been examined in laboratory studies [*Adams*, 1974, 1975; *Hunt and Salisbury*, 1970*a*,*b*; *Hunt et al.*, 1973] natural surfaces are rarely composed of a single mineral. Surfaces for which remotely sensed reflectance spectra are measured are more commonly composed of an assemblage of fine-grained intimately mixed minerals and alteration products. Determination of the proportions of minerals on these surfaces is important in understanding the geology and surface processes. Although this information pertaining to the composition is contained within reflectance spectra, one of the problems in reflectance spectroscopy is how to quantitatively determine mineral abundances from the reflectance spectrum of a natural surface, a mineral mixture.

Reflectance spectra of mineral mixtures are a systematic combination of the reflectances of pure mineral components or endmembers in the mixtures. Several investigators have examined the systematics theoretically and empirically and found that if the scale of mixing is large, or macroscopic, then the spectral systematics of mixing different materials are linear [*Singer and McCord*, 1979], while for microscopic or intimate mixtures the systematics are generally nonlinear [*Nash and Conel*, 1974; *Singer*, 1981]. To avoid the need to document the systematics of every possible intimate mixture series, a method that is general in approach and practical in application and also addresses the problem of nonlinear mixing is desired. A practical method for estimating mineral abundances has many powerful applications, especially with the advent of mapping spectrometers such as NIMS (on Galileo), AIS and AVIRIS (airborne), and VIMS (Mars Observer). The spatial and spectral (hence compositional) data obtained by these instruments will permit the mapping of surface mineralogy over broad regions. Presented here is a review of some of the present approaches to the problem of estimating mineral abundances from reflectance spectra of mineral mixtures and a revised model is derived. The accuracy of the revised model in predicting the endmember abundances in mixtures is tested with bidirectional reflectance spectra of mineral and soil mixtures where the grain size and composition of the mixtures are controlled. It is found that this approach predicts the relative contributions of the endmembers in the mixtures to within 5%.

Paper number 6B7232.
0148-0227/87/006B-7232$05.00

BACKGROUND

Several theories based on scattering principals exist for describing the complex interaction of light with particulate media [e.g., *Kubelka*, 1948; *Aronson and Emslie*, 1973; *Hapke*, 1981; *Lumme and Bowell*, 1981]. These theories generally model the reflectance of a particulate surface as a function of variables related to (1) the physical state of the surface (particle size, surface roughness, etc.), (2) properties of the individual components comprising the surface (complex indices of refraction, absorption coefficients, etc.) and (3) viewing geometry or type of reflectance measured. In their most general form it is often impractical to apply the models directly to remote measurements since the derivation of all the parameters requires multiple viewing geometries. However, the equations may be simplified using first-order assumptions about the scattering

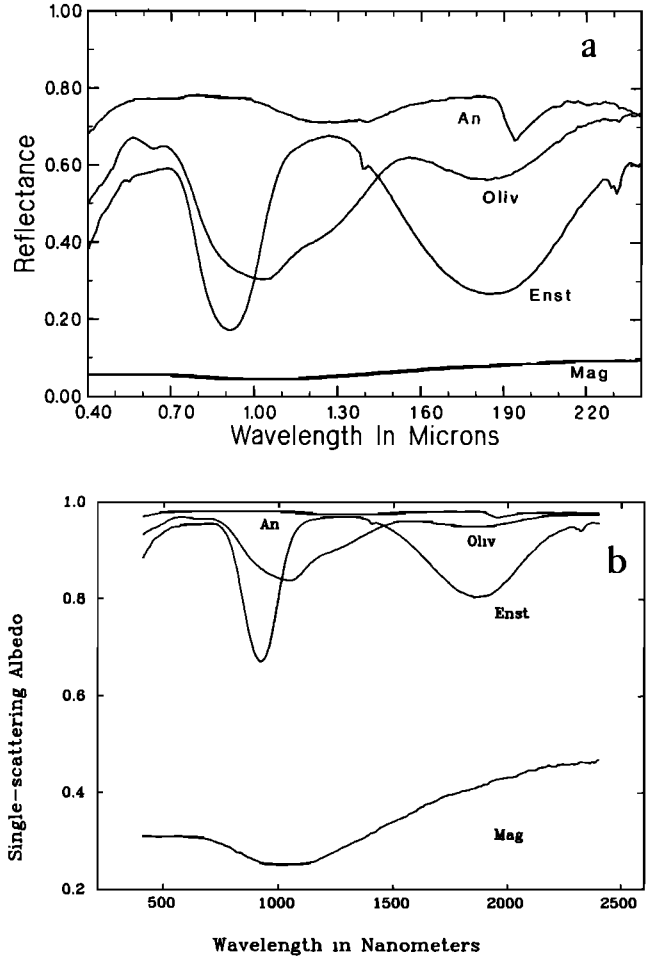

Fig. 1. (a) Reflectance spectra measured with an incidence angle of 30° and a vertical (0°) detection angle and (*b*) single-scattering albedo spectra computed from the reflectance spectra in (*a*) and equation (5) for the igneous rock-forming minerals anorthite (An), olivine (Oliv), enstatite (Enst), and magnetite (Mag) used in the mixing series analysis. Particle size used for these measurements is 45 to 75 μm.

properties of the surface such that abundance estimates may be obtained from a single viewing geometry.

Several investigators have developed practical approaches to the problem of nonlinear mixing of spectra in intimate mixtures by using combinations and variations of these models. *Johnson et al.* [1983] used a semiempirical mixing model based on the work of *Hapke* [1981] and the Kubelka-Munk equation [*Kubelka*, 1948; *Wendtland and Hecht*, 1966; *Kortum*, 1969]. In this model the mixing systematics are linearized by converting the measured direction-hemispherical reflectance spectra to single-scattering albedo (SSA) by the equation

$$R_H(\lambda) = [1 - (1 - w)^{1/2}] / [1 + 2\cos(i)(1 - w)^{1/2}] \quad (1)$$

where R_H is the directional-hemispherical reflectance, w is the mean SSA, and i is the incidence angle of the radiation. From *Hapke* [1981] it is predicted that the mean SSA of a mixture is a linear combination of the single-scattering albedos of the endmember components weighted by the relative geometric cross-section of that component. The equation describing this is

$$w(\lambda) = \Sigma w_n(\lambda)(M_n/\varrho_n d_n) / \Sigma(M_n/\varrho_n d_n) \quad (2)$$

where w is the mean SSA and w_n, M_n, ϱ_n, and d_n are the SSA, mass fraction, density, and particle diameter of component n, respectively. In both (1) and (2) it is assumed that the diameters of the particles in the mixtures are much greater than the wavelength of light and the particles have similar shapes. It follows that the coefficient by which the single-scattering albedo spectrum of component i in the mixture is weighted can be expressed as

$$F_i = (M_i/\varrho_i d_i) / \Sigma(M_n/\varrho_n d_n) \quad (3)$$

where F_i is the relative geometric cross-section for component i. When endmember particle sizes and densities are similar, the F-parameter values approximate the mass fractions of the endmembers in the mixtures. However, it is cautioned that the F-parameters cannot be directly interpreted without a priori information or assumptions concerning the particle diameters of the components in the mixtures.

Johnson et al. [1983] tested this approach on a suite of laboratory mixtures where the grain size, mass fraction, and purity of the endmembers in the mixtures were controlled. The SSA spectra of the pure mineral endmembers were combined to fit the spectra of the mixtures in a least squares sense. Although the fit of the endmembers to the mixture spectra were within experimental error, the predictions of F parameters were 2% to 30% from the actual values.

Recently, *Smith et al.* [1985] and *Johnson et al.* [1985] have applied principal components analysis (PCA) to a suite of laboratory and lunar spectra as an approach to understanding the systematics of intimate mixture spectra. They used this technique to identify the type of mixing (macroscopic versus microscopic), define the potential endmembers of the mixture, and estimate the relative proportions of endmembers in mixtures. Like the data used by *Johnson et al.* [1983], the reflectances were measured as or converted to directional-hemispherical reflectance. Spectra determined to be of intimate mixtures were converted to SSA using the technique of *Johnson et al.* [1983]. The power of their application of PCA is in the identification of endmembers from a group of spectra and the mixing relationships between spectra. However, the principal axes of variation require careful interpretation and the quantitative determination of endmember abundances for mixtures containing more than two components is complex.

MODEL

The approaches described in the previous section convert directional-hemispherical reflectances (the ratio of the radiant power scattered from a surface to the collimated light with a specific angle of incidence) to SSA to linearize the systematics of intimate mixtures. However, remotely sensed spectral data are most commonly measured as bidirectional reflectance (the reflectance of a surface illuminated by collimated light incident on the surface with an angle i and detected at a specific angle of emergence, e). An approach is therefore needed that is consistent with this type of reflectance measurement.

Hapke [1981] has developed a comprehensive series of solutions to the radiative transfer problem for particulate media. Among the derivations are a series of equations relating bidirectional reflectance, R, measured relative to a lambertian surface to the viewing geometry and parameters of a particulate medium. These are

TABLE 1. Actual and Computed Mass Fractions and F-Parameters Unconstrained

Actual				Computed				
Mass Fraction		F-Parameter		Mass Fraction		F-Parameter		SD*
Olivine	Anorthite							
90	10	0.879	0.121	88.6	11.4	0.862	0.136	1.2
75	25	0.707	0.193	69.7	30.1	0.649	0.349	0.9
50	50	0.446	0.554	54.1	45.9	0.487	0.513	1.0
25	75	0.211	0.789	23.6	76.2	0.119	0.799	0.5
10	90	0.082	0.918	09.8	90.2	0.081	0.919	0.5
Anorthite	Enstatite							
90	10	0.916	0.084	89.5	10.3	0.912	0.087	0.6
75	25	0.784	0.216	75.4	24.6	0.788	0.212	0.6
50	50	0.548	0.452	49.6	50.4	0.544	0.456	1.5
25	75	0.287	0.713	25.1	74.9	0.289	0.711	1.1
10	90	0.119	0.881	11.7	88.1	0.138	0.859	1.8
Olivine	Enstatite							
90	10	0.897	0.103	90.2	10.1	0.900	0.104	2.8
75	25	0.745	0.255	75.4	25.1	0.749	0.256	2.6
50	50	0.493	0.507	50.8	49.5	0.501	0.502	2.3
25	75	0.245	0.755	26.4	73.5	0.259	0.740	1.5
10	90	0.097	0.903	12.6	87.5	0.123	0.878	1.9
Olivine	Magnetite							
95	5	0.967	0.033	98.1	-2.8	0.988	-0.018	1.8
90	10	0.933	0.067	92.2	1.2	0.949	0.008	1.1
75	25	0.823	0.177	79.8	6.4	0.861	0.042	2.6
50	50	0.610	0.390	55.6	31.6	0.662	0.228	2.5
25	75	0.343	0.657	27.8	62.4	0.376	0.515	3.1
Sandstone	Gypsum†							
75	25	0.841	0.159	76.9	22.8	0.855	0.144	1.3
50	50	0.628	0.372	51.8	48.8	0.642	0.359	1.5
25	75	0.360	0.640	16.5	82.7	0.259	0.731	1.8
Sandstone	Kimberlite†							
75	25	0.776	0.224	73.3	26.7	0.760	0.240	0.7
50	50	0.537	0.463	48.9	50.7	0.525	0.471	1.2
25	75	0.279	0.721	26.7	73.7	0.296	0.708	3.2

* Standard deviation (x 10^{-3}).
† Calculated using wavelength region 0.6 to 2.4 mm.

$$R(i,e,g) = [w/4(\mu + \mu_o)][(1 + B(g))P(g) + H(\mu)H(\mu_o) - 1] \quad (4)$$

where $\mu_o = \cos(i)$, $\mu = \cos(e)$, g is the phase angle, B(g) is the backscatter function, P(g) is the single particle phase function, and H(μ) is Hapke's approximation to *Chandrasehkar's* [1960] equation to describe multiple scattering between particles. The H(μ) function is defined by

$$H(\mu) = (1 + 2\mu) / (1 + 2\mu\gamma)$$

where $\gamma = (1 - w)^{1/2}$.

In (4) variables pertaining to the scattering properties and compactness of the surface are contained within the functions P(g) and B(g). In order to solve for all the parameters a number of viewing geometries (i,e) are needed. This is impractical for most measurements made with remote detectors that have fixed viewing geometries. Viewing geometries most commonly employed by current airborne spectrometers have an emergence angle of 0° and incidence angles of 15° to 40°. For the purpose of deconvolving spectra into mineral abundances, the most important parameter is w (see equation (2)). Therefore it is desirable to simplify this equation so that w may be derived or approximated from bidirectional data obtained using a single viewing geometry.

The single particle phase function, P(g), describes the scattering properties of a particle as a function of phase angle. The function is approximated by a Legendre polynomial with coefficients b and c. These coefficients determine the shape of the function and may vary both with wavelength and composition. However, if the particles are assumed to be much larger than the wavelength of light and are randomly oriented on the surface, then to first order the surface scatters light isotropically [*Johnson et al.*, 1983]. For an isotropic surface, b = c = 0 and P(g) = 1 [*Hapke*, 1981].

The B(g) function describes the opposition effect, a surge in reflectance at small phase angles, and contains a regolith compaction parameter [*Hapke*, 1986]. The function is most important at small phase angles (<10°) and decays exponentially to near zero at 90°. If the assumption is made that B(g)<<1 at intermediate phase angles (between 15° and 40°), commonly used by imaging spectrometers, then (4) becomes

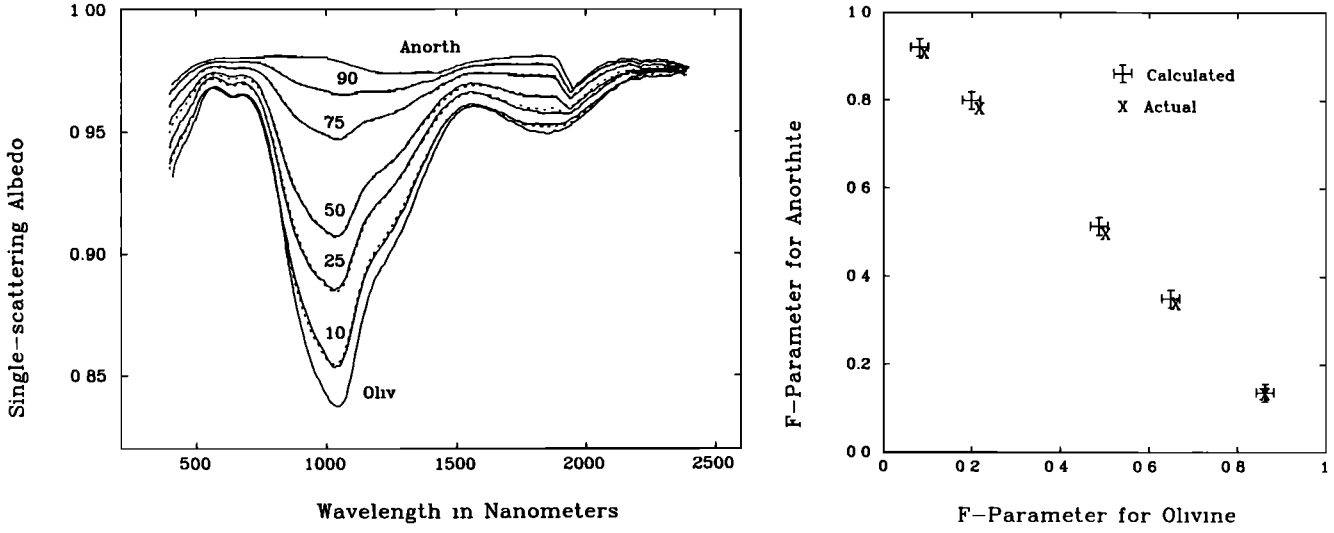

Fig. 2*a*.

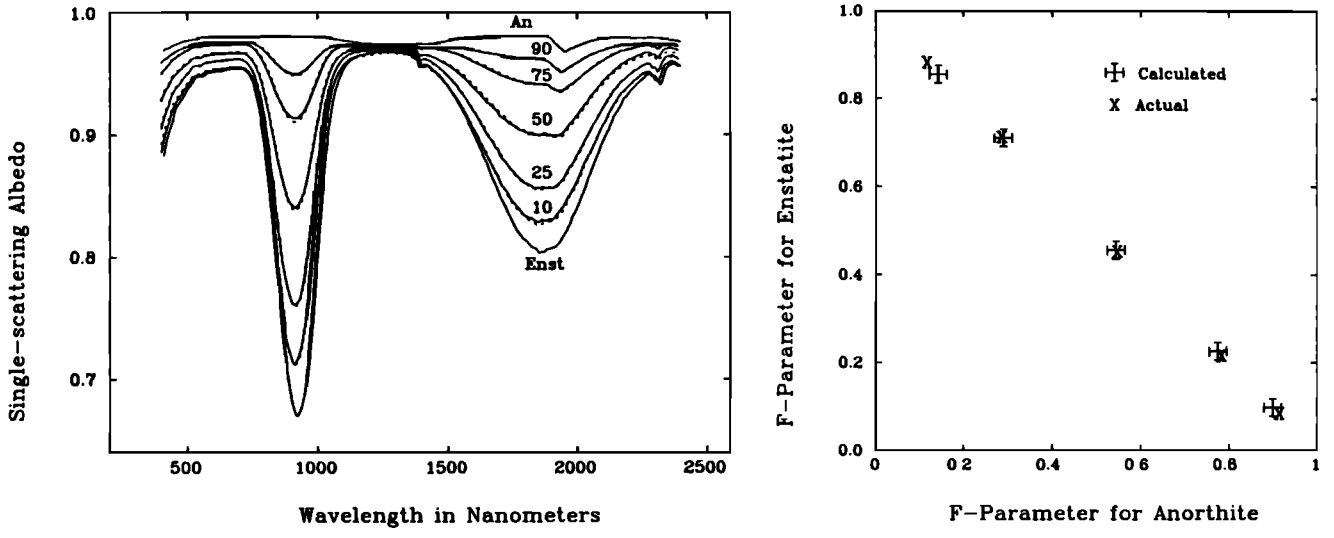

Fig. 2*b*.

Fig. 2. Single-scattering albedo (SSA) spectra measured at i = 30° and e = 0° and computed SSA spectra and predicted and computed relative geometric cross sections (F-parameter plots) for the mixture series (*a*) anorthite-olivine, (*b*) anorthite-enstatite, (*c*) olivine-enstatite, and (*d*) olivine-magnetite. Measured laboratory spectra are the solid lines and the calculated least squares fit of the endmember mineral spectra to the mixture spectra are the dotted curves. The endmember mineral spectra are labeled with the same letter codes as Figure 1, and the mixture spectra are labeled with numbers that refer to the mass fraction of the higher albedo component. Actual F-parameters are determined by the known mass fraction, particle size, and density of the components in the mixtures. The calculated F-parameters are determined from the least squares fit of the endmember spectra to the measured mixture spectra. Lines were added to emphasize the systematic offset between the actual and calculated F-parameters in plot (*d*).

$$R(i,e) = [\, w / 4(\mu + \mu_o)\,]\,[\, H(\mu)\, H(\mu_o)\,] \qquad (5)$$

Equation (5) is easily applied to bidirectional reflectance measurements to convert the reflectance data to SSA. In the following section, (5) will be used to derive SSA values used in the calculation of the F-parameters.

Experimental Analysis

The validity of (5) for deriving SSA from reflectance and (2) for describing the SSA spectra of intimate mixtures was tested on a series of laboratory mixtures of igneous rock-forming minerals and on a suite of mixtures of natural soils from a field area under study in southeastern Utah. The spectra were obtained from 0.4 to 2.4 μm with RELAB, a high-resolution, bidirectional reflectance spectrometer. The spectra are measured relative to the standard halon at the same viewing geometry (i = 30°, e = 0°) as the samples. Halon is an inert fluorocarbon and is nearly featureless at visible to near infrared wavelengths. It has an average reflectance >96% and can be approximated as an isotropic scatterer [*Pieters*, 1983]. Reflectance values measured relative to halon are then calibrated to the absolute reflectance

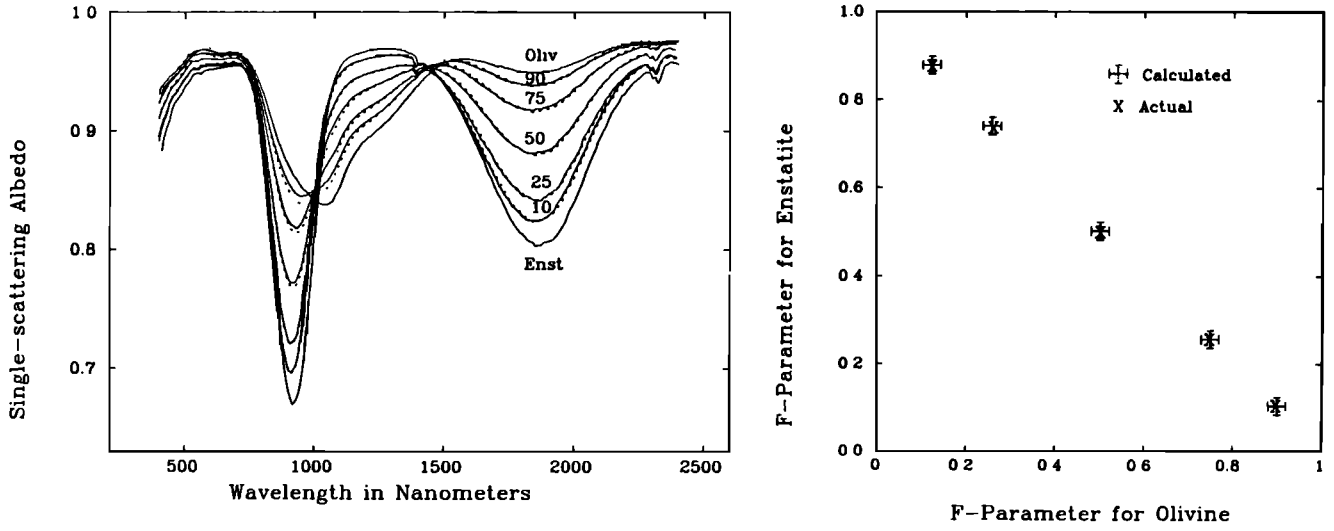

Fig. 2c.

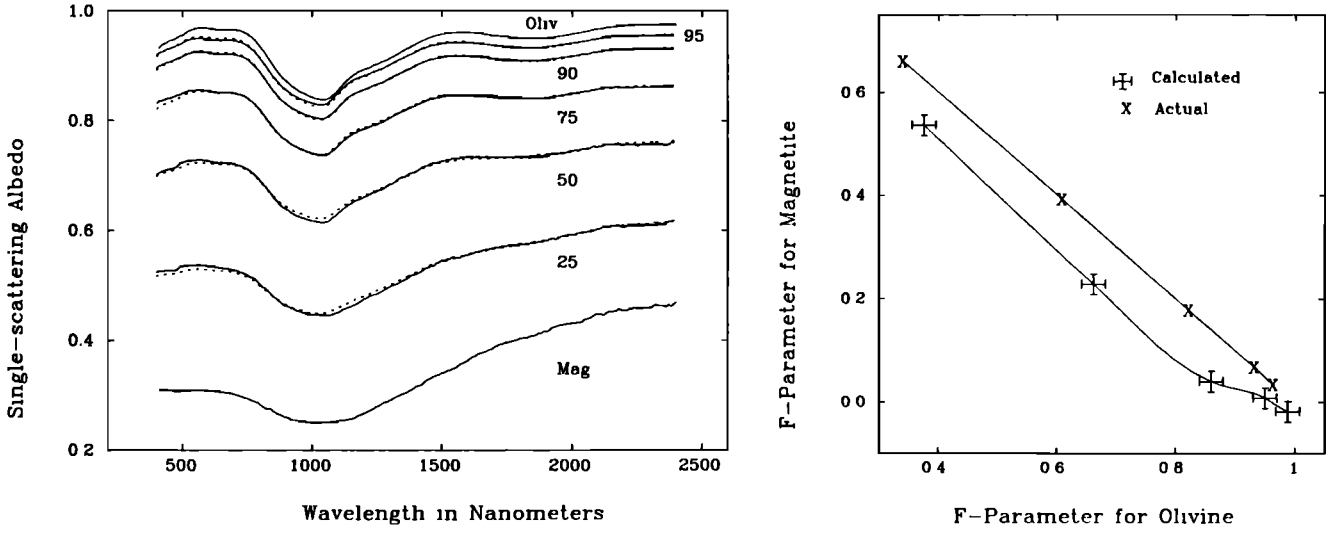

Fig. 2d.

Fig. 2. (continued)

of halon as determined by the National Bureau of Standards (National Bureau of Standards test 232.04/213408). These spectral measurements are to first order true or absolute bidirectional reflectances.

The minerals used for the rock-forming suite are anorthite, olivine, orthopyroxene (variety enstatite), and magnetite. RELAB spectra of these endmembers are shown in Figure 1 along with the SSA spectra computed using (5). The minerals are relatively homogeneous except for the olivine, which contains a 10–15% component of orthopyroxene as indicated by the small 2.0 μm absorption band. Because this is a general approach to the problem of nonlinear mixing this contamination will not effect the results.

The endmember minerals contain a variety of absorption features and contrasts in albedo and therefore provide a good test of the equations used to model intimate mixtures. The minerals were crushed and wet sieved with ethanol to the 45 to 75 μm particle size and then weighed and mixed in specific proportions. The endmember and mixture spectra were measured with RELAB using an incidence angle of 30° and a vertical emergence or detection angle. Each sample was measured twice to assure reproducibility. Although unpacking and repacking the samples can result in a 2% difference in reflectance, this was found to have little effect on the calculations.

The actual or expected relative geometric cross sections (equation (3)) were computed for the components of the mixtures from the mass fractions used in constructing the mixtures and the relative particulate densities measured in the laboratory. For a binary mixture the relative geometric cross section, F, is calculated from (3) where for component 1, $F_1 = (M_1/\varrho_1 d_1)/(M_1/\varrho_1 d_1 + M_2/\varrho_2 d_2)$ and for component 2, $F_2 = (M_2/\varrho_2 d_2)/(M_1/\varrho_1 d_1 + M_2/\varrho_2 d_2)$. These computed values are refered to as F_{ACTUAL} after *Johnson et al.* [1983]. Since the particle sizes for the igneous minerals were sieved to the same size fraction, the particle diameter term, d_i, is constant and can be removed from the equation.

TABLE 2. Actual and Computed Mass Fractions and F-Parameters Constrained so They add up to 1.0

Actual				Computed				
Mass Fraction		F-Parameter		Mass Fraction		F-Parameter		SD*
Olivine	Anorthite							
90	10	0.879	0.121	90.4	9.6	0.883	0.117	1.7
75	25	0.707	0.193	70.5	29.5	0.658	0.342	1.0
50	50	0.446	0.554	50.1	49.9	0.493	0.507	1.2
25	75	0.211	0.789	25.2	74.8	0.210	0.790	0.8
10	90	0.082	0.918	10.6	89.4	0.084	0.916	0.5
Anorthite	Enstatite							
90	10	0.916	0.084	88.4	11.6	0.903	0.097	1.2
75	25	0.784	0.216	75.8	24.2	0.791	0.209	0.7
50	50	0.548	0.452	50.1	49.9	0.548	0.452	1.5
25	75	0.287	0.713	25.2	74.8	0.290	0.710	1.1
10	90	0.119	0.881	10.6	89.4	0.125	0.875	2.5
Olivine	Enstatite							
90	10	0.897	0.103	92.3	7.7	0.921	0.079	4.8
75	25	0.745	0.255	77.6	22.4	0.771	0.229	4.9
50	50	0.493	0.507	52.6	47.4	0.519	0.481	4.1
25	75	0.245	0.755	26.4	73.6	0.259	0.741	1.5
10	90	0.097	0.903	13.8	86.2	0.135	0.865	2.9
Olivine	Magnetite							
95	5	0.967	0.033	95.7	4.3	0.972	0.028	3.2
90	10	0.933	0.067	89.0	11.0	0.927	0.073	3.9
75	25	0.823	0.177	72.0	28.0	0.801	0.199	9.0
50	50	0.610	0.390	48.4	51.6	0.595	0.405	10.3
25	75	0.343	0.657	22.3	77.7	0.310	0.690	10.7
Sandstone	Gypsum†							
75	25	0.841	0.159	77.2	22.8	0.856	0.144	1.5
50	50	0.628	0.372	50.5	49.5	0.634	0.366	13.2
25	75	0.360	0.640	17.4	82.6	0.271	0.729	9.4
Sandstone	Kimberlite†							
75	25	0.776	0.224	74.4	25.6	0.770	0.230	0.8
50	50	0.537	0.463	42.1	57.9	0.456	0.544	2.6
25	75	0.279	0.721	33.5	66.5	0.368	0.632	4.0

* Standard deviation (x 10^{-3}).
† Calculated using wavelength region 0.6 to 2.4 mm.

For each mixture SSA spectrum the endmember SSA spectra were combined linearly to fit the mixture spectrum in a least squares sense so as to minimize the variance between the measured and predicted curves. The proportion of each endmember SSA spectrum required to minimize the variance between the measured and computed mixture SSA spectra determine the calculated values of F or F_{CALC}. The quality of the fits is determined by calculating the standard deviation between the actual and calculated curves. The standard deviations are not greater than 4 x 10^{-3} in all cases and are approximately what is expected for experimental error.

The results for the analyses of mixtures of igneous rock forming minerals are shown in Table 1 and Figure 2 using equation (5) to derive SSA, equation (2) to calculate the F-parameters, and equation (3) to compute mass fractions. In Figure 2 the endmember SSA spectra, measured mixture spectra, and least squares fit spectra for each series are shown with a plot of the actual and calculated F-parameters. In the F-parameter plots, the sum of the F-parameters for any mixture should come to 1.0 and therefore plot along the line between 1.0 on the horizontal axis and 1.0 on the vertical axis.

Table 1 and the F-parameter plots in Figure 2 demonstrate that for most of these mixtures this method is valid for deriving accurate estimates of the abundances of minerals in the intimate mixtures to within 5% if endmember reflectance spectra and particle diameters are known. For the mixture series olivine-anorthite the computed abundances agree with the actual abundances to within 5% while agreements between F_{CALC} and F_{ACTUAL} for the olivine-enstatite and anorthite-enstatite mixture series are better than 3%.

For the olivine-magnetite series, however, the calculated values are not as accurate and the sum of the values of F_{CALC} for each mixture are less than 1.0 (Figure 2d). The mismatch is nevertheless systematic; an overprediction of the olivine content and an underprediction of the magnetite content. The fact that for mixtures containing magnetite, a strongly absorbing species, this sum is significantly less than 1.0 is valuable information that indicates that the model is inappropriate for magnetite-bear-

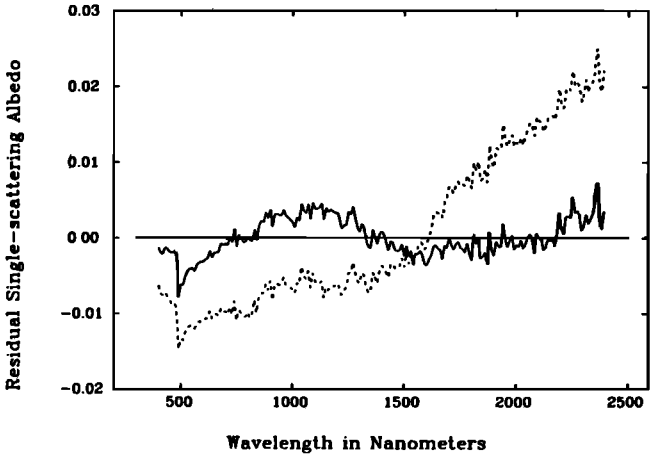

Fig. 3. Residual single-scattering albedo spectra (measured – predicted spectra) for the olivine-magnetite 50/50 mixture (see Figure 2*d*). The solid line is the residual for the unconstrained solution and the dashed line is for the constrained solution.

ing mixtures. The source for this error probably lies in the simplifying assumptions made concerning the single-particle phase function (P(g)) and/or the backscatter function (B(g)) and suggests that magnetite scatters light anisotropically and/or displays significant backscatter at 30°.

Since physically and by definition the F-parameters and mass fractions must sum to 1.0, these values were recalculated from the SSA spectra with the least squares approach using this constraint. The results are shown in Table 2. For the nonmagnetite-bearing mixtures, the changes in computed abundances are small. In about half of the cases the calculated abundances are in slightly better agreement with the actual abundances while the reverse holds true for the rest. The error of the least squares fit is increased up to a factor of 2 over the unconstrained case. For the olivine-magnetite mixtures the calculated abundances when the F-parameters are forced to sum to unity are in significantly better agreement (to within 3%) but the error of the fit is 2 to 4 times worse than the unconstrained fits. The residuals, or magnitude of the misfit between the actual SSA and the least squares fit SSA, can be examined as a function of wavelength. In Figure 3 are shown the residual SSA spectra for the olivine-magnetite 50/50 mixture in the constrained and unconstrained cases. The residual in the constrained case exhibits systematic errors with wavelength implying departure from the desired fitting of diagnostic features. In the nonmagnetite mixtures the constrained residual spectra are generally the same shape as the unconstrained residual spectra but are usually offset from the unconstrained residual spectra and show greater variation along the residual axis. Although the agreement between actual and calculated abundances in some cases appear to be improved by using the constrained solution, the unconstrained solutions are more sensitive to spectral variations, provide a check on the assumptions and mineral components used in the model, and provide information on the systematics of the error in cases where the model is inappropriate.

The method of estimating abundances presented here should be independent of the composition of the endmembers. That is, if the endmembers chosen are the primary components of a mixture then it should be possible to deconvolve the spectrum of a mixture into the endmember abundances. In remote sensing applications it is commonly difficult to uniquely identify all endmember minerals or to extract the relative importance of rock coatings such as amorphous iron oxide gels. However, it is often possible to define common assemblages of minerals or minerals and coatings. For such occurrences it would be desirable to treat the complex assemblages as endmembers themselves.

Mixture series of natural soils were made to explore this possibility. The soils were collected from southeastern Utah as part of ongoing research with imaging spectrometers. Endmember soils from this site were chosen that are important surface components for understanding the mixing systematics in the area under investigation. The endmember soils for the mixtures consist of (1) a reddish-brown soil derived from the weathering of a similar colored sandstone, (2) a relatively pure gypsum commonly found in the sedimentary sequences in this region, and (3) the weathered derivative of a kimberlite. The sandstone soil was dry sieved to the 45 to 75 μm size fraction and the other soils were sieved to the 75 to 125 μm particle size prior to mix-

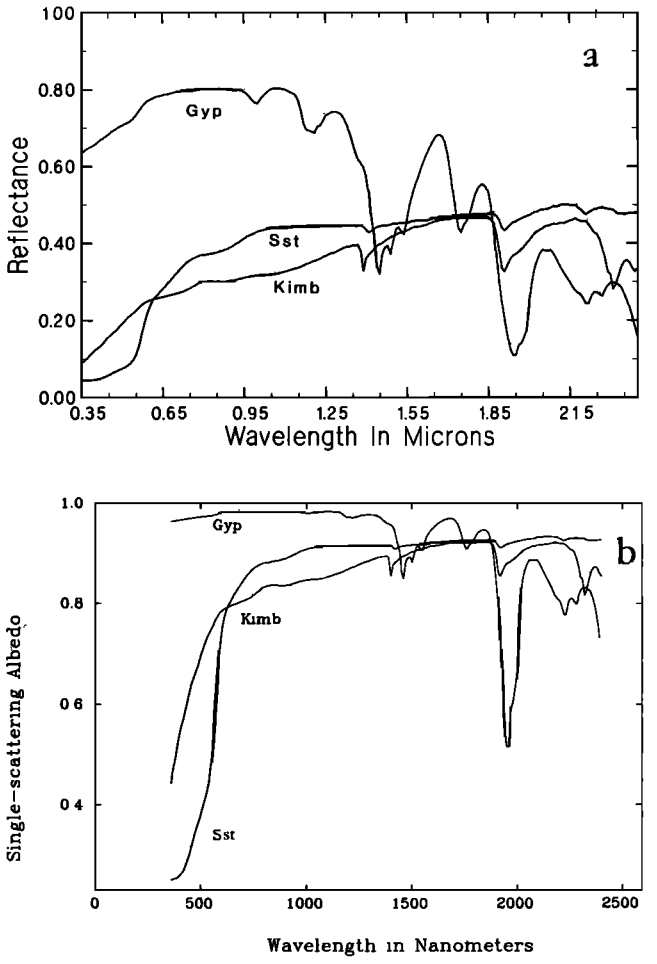

Fig. 4. (*a*) Reflectance spectra measured with an incidence angle of 30° and a vertical (0°) detection angle and (*b*) single-scattering albedo spectra computed from the reflectance spectra in (*a*) using equation (5) for the terrestrial desert soils containing gypsum (Gyp), sandstone (Sst), and kimberlite (Kimb) used in the mixing series analysis of complex endmember mixing.

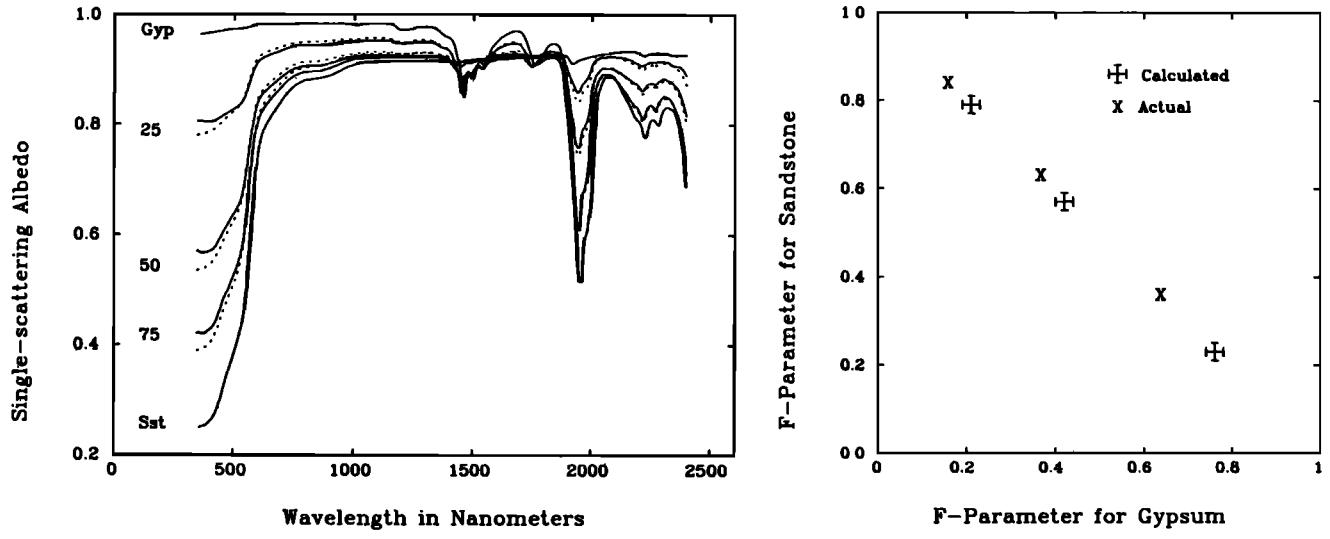

Fig. 5*a*.

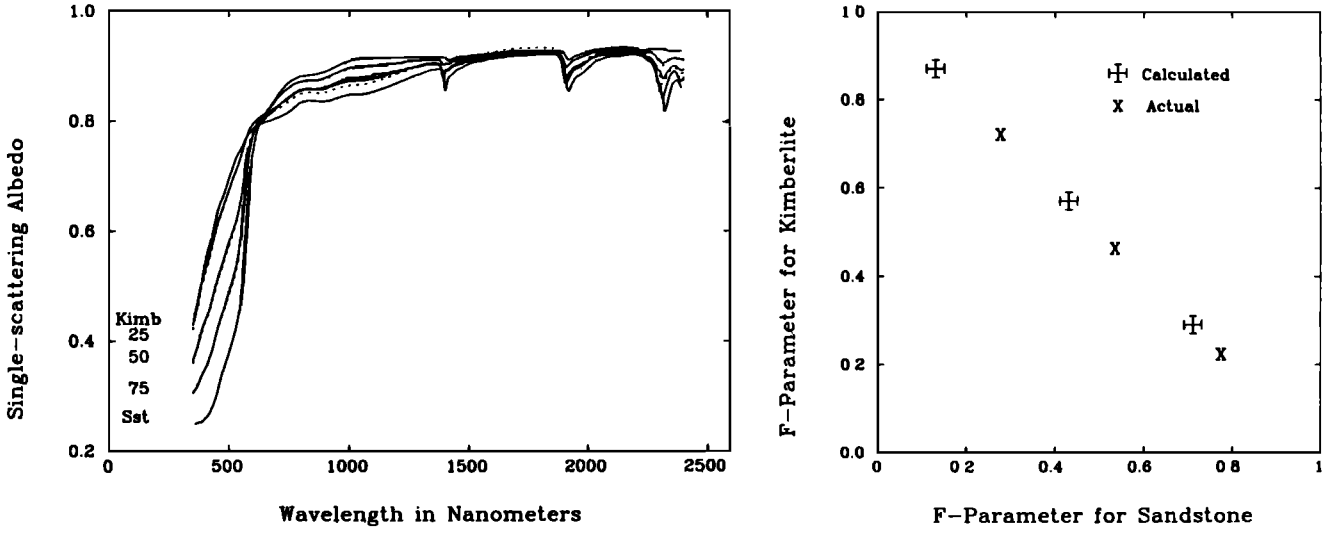

Fig. 5*b*.

Fig. 5. Results of mixture series analysis of complex endmembers using the wavelength region 400 to 2400 nanometers. The plots are presented as in Figure 2. The numbers in the spectral plots refer to the mass fraction of sandstone in the (*a*) gypsum-sandstone and (*b*) kimberlite-sandstone mixture series.

ing. When viewed under a binocular microscope the gypsum and sandstone soils were generally clean, single particles. However, many of the particles in the kimberlite soil were clumps of smaller particles. The clumped particles behave as strong internal scatters and reduce the effective particle size of this sieve fraction. RELAB reflectance spectra of the soils and SSA spectra for the same soils are shown in Figure 4. In the spectrum of the sandstone soil the presence of ferric iron oxide is evidenced by the strong charge transfer bands at visible wavelengths. The gypsum spectrum shows well-defined OH^- and H_2O overtone bands near 1.4, 1.6, and longward of 1.8 μm. The kimberlite spectrum contains Fe^{2+} and Fe^{3+} absorptions at 0.7, 0.9, and 1.1 μm and OH^- and H_2O overtone bands at 1.4 μm and longward of 1.8 μm.

The results of deconvolving the spectra of the mixtures for the natural soil mixtures are shown in Figure 5. It is immediately evident in the F-parameter plot that the values of F_{CALC} are in relatively poor agreement with F_{ACTUAL} for both of the mixture series. The mismatches are systematic and in both cases there is an underprediction of the sandstone component and an overprediction of the complimentary component. It is observed in Figure 5*a* that the greatest mismatch between observed and predicted mixture spectra occurs in the wavelength region 0.4 to 0.6 μm. This suggests that this wavelength region, where the sandstone is strongly absorbing, may contain the cause of the systematic error. To test this presumption, selected portions of the spectra were deconvolved separately. Significantly different results were obtained when using the wavelengths shorter than 0.6 μm (the shoulder of the strong charge transfer bands) than when using wavelengths longer than 0.6 μm.

In Figure 6 are plotted the values of F_{CALC} computed from using only the wavelength regions 0.4 to 0.5 μm and 0.4 to 0.6

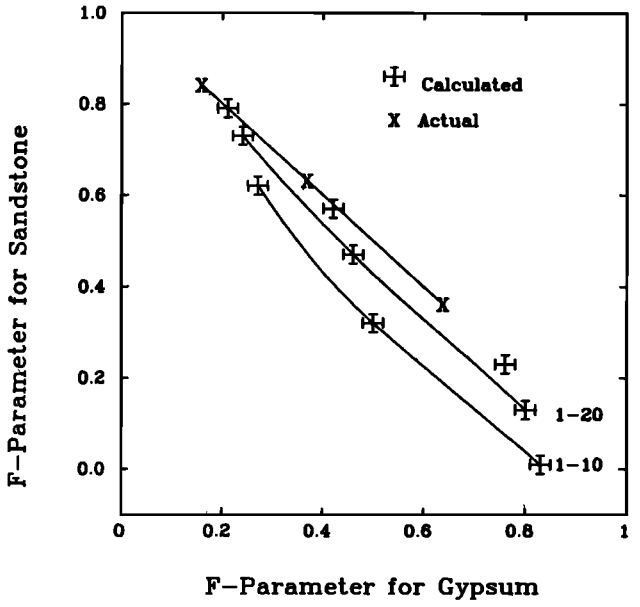

Fig. 6. F-parameter plot for the selective deconvolution of the gypsum-sandstone mixture series. The unconnected calculated values are from using the whole spectrum from 400 to 2400 nanometers and the connected calculated values are from deconvolving the wavelength regions 0.4 to 0.5 μm (1–10) and 0.4 to 0.6 μm (1–20) of the spectra in Figure 5*a*. This wavelength region shorter than 600 nanometers includes the strong charge transfer bands in the sandstone spectrum.

μm in the sandstone-gypsum mixtures and appropriate endmembers. In this wavelength region (0.4 to 0.6 μm), the sandstone spectrum is dominated by the strong iron oxide absorptions. Not only is the same systematic underprediction of the sandstone and overprediction of the gypsum observed but the sum of the F-parameters are less than 1.0. These systematics, similar to those observed for the olivine-magnetite mixture series, occur in the spectral region where the sandstone soil is strongly absorbing. The mismatches are most severe where the reflectances of the strongly absorbing component are less than 10%. These values of F_{CALC} using the visible portion of the spectrum converge to the values obtained from using the whole spectrum as increasing portions of the spectrum are used. Therefore the mismatch in F-parameters of the whole spectrum is apparently controlled by the wavelength region where the particles are strongly opaque.

The results from using those wavelengths longward of the charge transfer bands to deconvolve the gypsum-sandstone mixture spectra are shown in Table 1 and Figure 7*a*. This strategy clearly provides a more acceptable prediction of F-parameters and hence endmember abundances. In Figure 7*b* and Table 1 are plotted the values calculated from deconvolving those wavelengths longward of the charge transfer bands for the kimberlite-sandstone mixtures and again one sees a much better agreement between actual and calculated values. Table 2 contains the complex mixture deconvolution results for the constrained case. Although the abundances calculated for the sandstone-gypsum series show little change from the unconstrained solution, the residual errors are once again higher. A much worse agreement is observed in the constrained case between actual and predicted abundances for the sandstone-kimberlite series.

These results show that the assumption and equations presented are valid for the wavelength region where the components do not behave as strongly absorbing particles. The exact limit of reflectance where the model breaks down is not possible to define given the present data set, but certainly reflectances >25–30% respond well to this model while components with reflectances <10% result in less accurate F-parameter predictions.

SUMMARY AND CONCLUSIONS

The bidirectional reflectance equations of *Hapke* [1981] were used as an approach to estimating mineral abundances from reflectance spectra. The equations were simplified by the

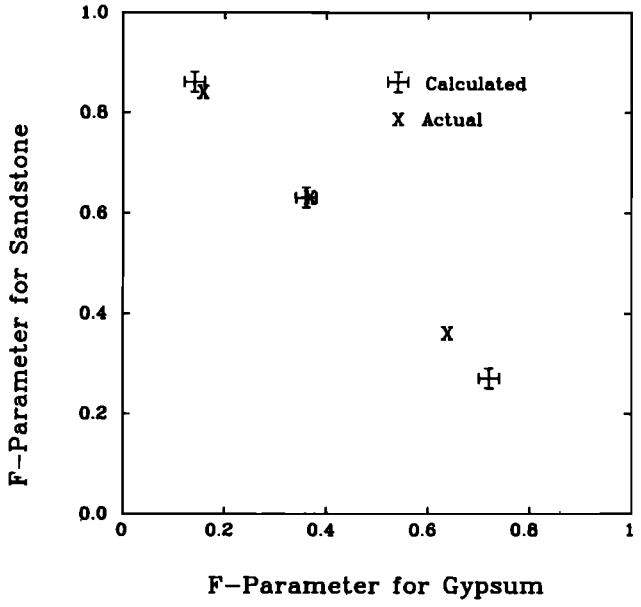

Fig. 7*a*.

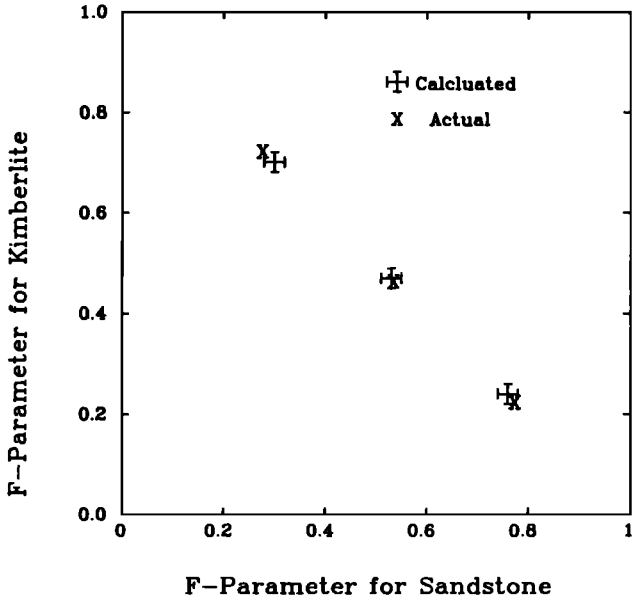

Fig. 7*b*.

Fig. 7. F-parameter plots for (*a*) gypsum-sandstone and (*b*) kimberlite-sandstone mixture series where the calculated values are from deconvolving the mixture spectra shown in Figure 6 from 800 to 2400 nanometers, longward of the strong charge transfer bands in the sandstone spectrum.

assumption that at intermediate phase angles, most surfaces scatter light isotropically. In order to obtain mineral abundances this approach requires the reflectance spectra of the endmembers as well as some knowledge or estimate of the particle sizes of the endmembers. The technique presented here was used to deconvolve bidirectional reflectance spectra of intimate mineral mixtures into the relative proportions of the endmembers in the mixtures. Mass fractions of the mineral components were calculated to within 5% for most, and within 8% for all the mixtures without strongly absorbing components. For mixtures that contain more than several percent low albedo material (<10% reflectance), or for wavelength regions where components behave as strongly absorbing particles, a somewhat modified version of this approach will need to be developed. The endmembers need not be pure mineral components since the technique is also valid when complex intimate mixtures are used as endmembers, but the choice of appropriate endmembers is an important consideration. They may be chosen from a library of spectra and a priori knowledge about the surface, derived from detailed analysis of individual spectra from the data, or, for larger data sets, determined from mathematical transformations such as principal components analysis [e.g. *Smith et al.*, 1985].

If the restrictions concerning low albedo components are not a factor or can be accommodated (such as including the low albedo component in a complex mixture used as an endmember), this technique has many powerful applications. It is easily expanded for use with multicomponent problems and since abundances were calculated using a noniterative approach, this method is especially efficient for large spectral datasets such as those produced by mapping spectrometers (e.g., NIMS, VIMS, AVIRIS). Further work is required to determine the effects of varied particle sizes and to refine the assumptions to include strongly opaque components.

Acknowledgments. We wish to thank Paul Helfenstein for many useful discussions and Steve Pratt for technical assistance in obtaining the spectral measurements. We are also grateful to P. E. Johnson, B. Hapke, and T. Roush whose comments and suggestions have helped to improve this paper. This research was supported under NASA grant NASW-4048. RELAB is supported as a NASA facility under grant number NAGW-748.

REFERENCES

Adams, J. B., Visible and near-infrared diffuse reflectance: Spectra of pyroxenes as applied to remote sensing of solid objects in the solar system, *J. Geophys. Res.*, *79*, 4829–4836, 1974.

Adams, J. B., Interpretation of visible and near-infrared diffuse reflectance spectra of pyroxenes and other rock forming minerals, *Infrared and Raman Spectroscopy of Lunar and Terrestrial Materials*, edited by C. Karr, pp. 91–116, Academic, New York, 1975.

Aronson, J. R., and A. G. Emslie, Spectral reflectance and emittance of particulate materials, 2, Application and results, *Appl. Opt.*, *12*, 2573–2584, 1973.

Burns, R. G., *Mineralogical Application to Crystal Field Theory*, Cambridge University Press, London, 224 pp., 1970.

Chandrasekhar, S., *Radiative Transfer*, Dover, New York, 393 pp., 1960.

Hapke, B., Bidirectional reflectance spectroscopy 1. Theory, *J. Geophys. Res.*, *86*, 3039–3054, 1981.

Hapke, B., Bidirectional reflectance spectroscopy 4. The extinction coefficient and the opposition effect, *Icarus*, *67*, 264–287, 1986.

Hunt, G. R., and J. W. Salisbury, Visible and near-infrared spectra of minerals and rocks: I Silicate minerals, *Mod. Geol.*, *1*, 283–300, 1970*a*.

Hunt, G. R. and J. W. Salisbury, Visible and near infrared reflectance spectra of minerals and rocks: II Carbonates, *Mod. Geol.*, *2*, 23–30, 1970*b*.

Hunt, G. R., J. W. Salisbury, and C. J. Lenhoff, Visible and near infrared spectra of minerals and rocks: VI. Additional silicates, *Mod. Geol.*, *4*, 85–106, 1973.

Johnson, P. E., M. O. Smith, S. Taylor-George, and J. B. Adams, A semi-empirical method for analysis of the reflectance of binary mineral mixtures, *J. Geophys. Res.*, *88*, 3557–3561, 1983.

Johnson, P. E., M. O. Smith, and J. B. Adams, Quantitative analysis of planetary reflectance spectra with principal components analysis, *Proc. Lunar Planet. Sci. Conf. 15th*, in *J. Geophys. Res.*, *90*, C805–810, 1985.

Kortum, G., *Reflectance Spectroscopy*, Springer-Verlag, New York, 366 pp., 1969.

Kubelka, P., New contribution to the optics of intensely light scattering materials, 1, *J. Opt. Soc. Am.*, *38*, 448–457, 1948.

Lumme, K., and E. Bowell, Radiative transfer in the surfaces of atmosphereless bodies; I; Theory, *Astron. J.*, *86*, 1694–1704, 1981.

Nash, D. B., and J. E. Conel, Spectral reflectance systematics for mixtures of powdered hypersthene, labradorite, and ilmenite, *J. Geophys. Res.*, *79*, 1615–1621, 1974.

Pieters, C. M., Strength of mineral absorption features in the transmitted component of near-infrared reflected light: First results from RELAB, *J. Geophys. Res.*, *88*, 9534–9544, 1983.

Singer, R. B., Near-infrared spectral reflectance of mineral mixtures: Systematic combinations of pyroxenes, olivine, and iron oxides, *J. Geophys. Res.*, *86*, 7967–7982, 1981.

Singer, R. B., and T. B. McCord, Mars: Large scale mixing of bright and dark surface materials and implications for analysis of spectral reflectance, *Proc. Lunar Planet. Sci. Conf. 10th*, 1835–1848, 1979.

Smith, M. O., P. E. Johnson, and J. B. Adams, Quantitative determination of mineral types and abundances from reflectance spectra using principal components analysis, *Proc Lunar Planet. Sci. Conf. 15th*, in *J. Geophys. Res.*, *90*, C797–804, 1985.

Wendtland, M., and H. Hecht, *Reflectance Spectroscopy*, John Wiley, New York, 298 pp., 1966.

J. F. Mustard and C. M. Pieters, Department of Geological Sciences, Box 1846, Brown University, Providence, RI 02912.

(Received April 29, 1986;
revised October 10, 1986;
accepted February 11, 1987.)